Microscopic theory of magnetic phase transitions in $HoNi_2B_2C$

A. Amici
Max-Planck-Institut für Physik komplexer Systeme, 01187 Dresden, Germany

P. Thalmeier
Max-Planck-Institut für Chemiche Physik fester Stoffe, 01187 Dresden, Germany

(Received 26 June 1997; revised manuscript received 28 January 1998)

We present a microscopic theory for the low-temperature metamagnetic phase diagram of $HoNi_2B_2C$ that agrees well with experiments. For the same model we determined the zero-field ground state as a function of temperature and found the c-axis commensurate-to-incommensurate transition in the expected temperature range. The complex behavior of the system originates from the competition between the crystalline electric field and the Ruderman-Kittel-Kasuya-Yosida interaction, whose effective form is obtained. No essential influence of superconductivity has to be invoked to understand the magnetic phase diagram of this material. [S0163-1829(98)10217-5]

The recent interest in $HoNi_2B_2C$ and similar borocarbide compounds is motivated by the possibility of a detailed study of the mutual interaction between superconductivity (SC) (Ref. 1) and magnetic order (MO) (Refs. 2 and 3) coexisting in a few of these materials as bulk properties. The superconducting critical temperature for $HoNi_2B_2C$ is $T_c=8$ K (Ref. 1) and the upper critical field H_{c2}^{sc} is about $2\sim3.5$ kG.[4] Temperature-dependent measurements show a pronounced anomaly of $H_{c2}^{sc}(T)$ around 5 K that nearly leads the material to reentrance into the normal state.[2,5] In the same temperature range several magnetically ordered structures are observed in the Ho f electrons sublattice: a commensurate (C) antiferromagnetic phase below 5 K,[2,3] an incommensurate (IC) c-axis complex spiral state ($5\text{ K}<T<6\text{ K}$) (Refs. 3,6 and 7) and an a-axis IC modulation in a narrow range of temperature around 5.5 K.[6,8] Although no satisfactory theory is available presently, many experiments point to a correlation between this complex magnetic phase diagram and the SC anomalies.[9,10] Much insight on the magnetism of this material can be gained from a number of experiments reporting metamagnetic transitions at low temperature and fields higher than H_{c2}^{sc}.[2,11] In particular, the detailed anisotropic metamagnetic phase diagram at $T=2$ K presented in Ref. 12, can be used to extract many features of the magnetic interaction. In this work we propose a realistic microscopic model for the Ho $4f$-electrons subsystem of $HoNi_2B_2C$ that reproduces the main features of the low-temperature metamagnetic phase diagram as well as the zero-field sequence of phases as a function of temperature. It is important to note that many physical elements need to be included in the present theoretical description to have reasonable agreement with experiments and a model of a comparable complexity is needed to treat the mutual interaction between SC and MO.

The coexistence and weak coupling of the two phenomena of SC and MO is due to the different degrees of localization of electrons in the borocarbides. Local-density approximation calculations show that the conduction band is composed mainly of Ni $3d$ electrons,[13] which undergo the superconducting transition. On the other hand, magnetic properties are related to the well localized electrons in the incomplete $4f$ shell of Ho. The exchange interaction between these two electron systems is mediated by the small fraction of Ho $6s$ and $5d$ character in the conduction band. As far as magnetic properties are concerned, the conduction electrons can be eliminated in a standard way leading to an effective Ruderman-Kittel-Kasuya-Yosida (RKKY) exchange interaction among the stable Ho $4f$ moments. The appropriate Hamiltonian is then given by:[14]

$$\mathcal{H}=\sum_i \left[\mathcal{H}_{cf}(\mathbf{J}_i)-\boldsymbol{\mu}_i\cdot\mathbf{B}\right]-\frac{1}{2}\sum_{ij}\mathcal{J}(i,j)\ \mathbf{J}_i\cdot\mathbf{J}_j\,. \qquad (1)$$

This Hamiltonian includes the crystalline electric field (CEF) single-ion part $\mathcal{H}_{cf}(\mathbf{J}_i)$ expressed in terms of the total angular momentum $\mathbf{J}_i$, the Zeeman interaction between the local magnetic induction $\mathbf{B}$ and the magnetic moment $\boldsymbol{\mu}_i=\mu_B g\mathbf{J}_i$ (μ_B is the Bohr magneton and $g=\frac{5}{4}$, the gyromagnetic ratio for Ho), and the effective RKKY exchange interaction. The direct dipole-dipole interaction is not relevant in borocarbides[15] and this allows us to use a magnetic induction field $\mathbf{B}$ independent of the position. The CEF single-ion Hamiltonian we use is the one extracted from neutron-diffraction experiments in Ref. 16 and contains no adjustable parameter. Its ground state is a Γ_4 singlet and the first exited states are a Γ_5^* doublet at 0.15 meV from the ground state and a Γ_1 singlet at 0.32 meV. The other 13 CEF states have much higher excitation energies (>10 meV) and their matrix elements with the low-energy quartet is very small, therefore they may be neglected in the whole range of temperature and fields that we explored. Regarding the magnetic interaction, no previous knowledge is available about the RKKY function $\mathcal{J}(i,j)$ and an important aim of this work is to obtain a realistic model for it.

Since we are dealing with a three-dimensional system of large angular momenta ($J_{Ho}=8$) it is possible to treat its Hamiltonian at a mean-field (MF) level. Introducing the mean thermal value $\langle\mathbf{J}_i\rangle$ and neglecting the terms containing

the two sites' fluctuations, it is possible to decouple the dynamics of the different sites. The single-ion MF Hamiltonian is then given by:[14]

$$\mathcal{H}_{mf}(i)=\mathcal{H}_{cf}(\mathbf{J}_i)-\mathbf{J}_i\cdot\mathbf{B}_i^e+\mathcal{E} \tag{2}$$

in which $\mathbf{B}_i^e=(\mu_B g\mathbf{B}+\Sigma_j\mathcal{J}(i,j)\langle\mathbf{J}_j\rangle)$ is the effective molecular field and $\mathcal{E}=\frac{1}{2}\langle\mathbf{J}_i\rangle\Sigma_j\mathcal{J}(i,j)\langle\mathbf{J}_j\rangle$. The diagonalization of this single-site Hamiltonian can be easily achieved numerically. The single-ion Gibbs free-energy density F_i^M and the corresponding average angular momentum $\langle\mathbf{J}_i\rangle$ can be computed as functions of $\mathbf{B}_i^e$ and T. This leads to the self-consistent MF equations for the $\langle\mathbf{J}_i\rangle$ that can be solved iteratively. Two experimental evidences can be used to reduce the number of independent sites whose MF magnetization should be computed. First of all, almost all the observed structures in this compound share the property of ferromagnetic alignment in the ab plane. The only exception is the a-axis modulation whose structure is not yet clear. However, it appears not to coexist microscopically with the c-axis ones[7] and we will neglect it. Therefore we impose ferromagnetic alignment in the plane from the beginning, thus reducing the calculation to one dimension. Then the RKKY interaction has only c-dependence and, taking the magnetic moment in the site 0 as the reference, it may be parametrized with the help of $\mathcal{J}_i=\Sigma_{\{j_i\}}\mathcal{J}(0,j_i)$, with j_i running on all the sites of the ith plane. The $\mathcal{J}_i$ with $i\geqslant 1$ are the interaction of the reference moment with those in the neighboring layers and $\mathcal{J}_0$ is the interaction with the other moments in the same plane. The second simplification is related to the CEF structure, in fact the c-axis is a very hard direction in the whole range of temperature we are interested in, therefore we force the moments to lie in the ab plane neglecting their small out-of-plane component.

In order to establish the actual MF ground configuration for the $\langle\mathbf{J}_i\rangle$ out of the possible stable ones, we introduce the Helmholtz free-energy (HFE) density given by

$$F(\mathbf{r})=F^M(\mathbf{B})+\frac{B^2}{8\pi}-\frac{\mathbf{H}\cdot\mathbf{B}}{4\pi}=F^M(\mathbf{B})-2\pi M^2-\frac{H^2}{8\pi}, \tag{3}$$

with $\mathbf{B}(\mathbf{r})=\mathbf{H}(\mathbf{r})+4\pi\mathbf{M}(\mathbf{r})$.[17] The integral of $F(\mathbf{r})$ over all space is the proper thermodynamic function to be minimized when external fields are kept constant.[17] The magnetization contribution ($\sim$10 kG) is not negligible with respect to the typical external field (4–25 kG). However, the full problem of solving for $\mathbf{M}(\mathbf{r})$ in a finite sample with a given geometry is beyond our purpose. This is indeed a typical problem in the thermodynamics of magnetic materials[17] whose most practical solution is to assume cylindrical symmetry around the external field $\mathbf{H}$ in order to eliminate the spatial dependence of both $\mathbf{B}$ and $\mathbf{M}$. The homogeneous magnetization of the sample is calculated as $\mathbf{M}=g\mu_B/V_c\overline{\langle\mathbf{J}_i\rangle}$ where $V_c=65$ Å^3 is the volume of the unit cell and the bar indicates the average on all ions. Similarly, the contribution of the magnetization to the HFE per unit cell can be written as $2\pi M^2V=2\pi(g\mu_B)^2/V_c\overline{\langle\mathbf{J}_i\rangle^2}$.

Until now the actual RKKY interaction among magnetic moments remained unspecified. In order to achieve a convenient parametrization for it, we make extensive use of the $T=2$ K magnetization data in Ref. 12. From the clear presence of a flat magnetization plateau and from the value of the magnetization as a function of the angle, we argue that the magnetic moments of the ions are almost at the saturation value $J_s=J_{Ho}=8$ and they are locked in one of the four equivalent $\langle 110\rangle$ in-plane easy directions.[12] The sharp metamagnetic transitions are then due to first-order transitions among different arrangements of the moments along the c axis. We assume that the relevant phases in the field-angle phase diagram are the easiest commensurate structures with the observed magnetization (they are listed in the upper part of Table I). We notice that all the phases in Table I may be represented in a chain of six unit cells with periodic boundary conditions. This is important because the Fourier transform of the interaction for a system with six sites has only four free parameters, namely, $\mathcal{J}_i$ with i = 0, 1, 2, 3. Any further Fourier component may be removed with a redefinition of these parameters (i.e., the $\mathcal{J}_6$ is equivalent to $\mathcal{J}_0$). Neglecting the CEF energy and entropy it is possible to calculate analytically the HFE for each configuration. Some of these energies are listed in Table I. From the two $\theta=0°$ metamagnetic transitions it is possible to establish two conditions for the parametrization of the RKKY interaction. Following the convention of Canfield *et al.*[12] we call the metamagnetic transition fields $H_{c1}=4.1$ kG and $H_{c2}=11.1$ kG (this value is somewhat higher than the 10.6 kG given in Ref. 12), and they should not be confused with the superconducting critical fields. Imposing the energy of the $AF2$ and $AF3$ phases to be equal at H_{c1} and the ones of $AF3$ and P at H_{c2}, we obtain the following relations:

TABLE I. Stacking sequence of ferromagnetically ordered ab planes along the c axis for the phases found in the T = 2 K magnetic anisotropic phase diagram in Fig. 2. At low temperature the CEF forces the moments to lie in one of the four easy directions $\langle 110\rangle$ indicated by arrows. The external field forms an angle θ with the (−1,1,0) (↖) direction. The third column is the relevant part of the HFE per site, the term $-J_s^2\mathcal{J}_0/2-H^2/8\pi$ may be added to have the total HFE. $H_\parallel=g\mu_BH\cos(\theta)$ is the projection of the field along the easy axis and all other symbols are explained in the text. We only give the HFE for the phases needed to compute the relations (4).

Phase	Structure	HFE per site
P	↖	$-J_s^2(\mathcal{J}_1+\mathcal{J}_2+\mathcal{J}_3+E_M)-J_sH_\parallel$
AF2	↖↘	$J_s^2(\mathcal{J}_1-\mathcal{J}_2+\mathcal{J}_3)$
AF2′	↗↙	$J_s^2(\mathcal{J}_1-\mathcal{J}_2+\mathcal{J}_3)$
AF3	↖↘↖	$[J_s^2(\mathcal{J}_1+\mathcal{J}_2-3\mathcal{J}_3-E_M/3)-J_sH_\parallel]/3$
AF3′	↖↗↙	$[J_s^2(\mathcal{J}_1+\mathcal{J}_2-3\mathcal{J}_3-E_M/3)-J_sH_\parallel]/3$
F3	↖↗↖	
F2	↖↗	
C6	↖↘↖↗↙↗	

$$\mathcal{J}_1=-\mathcal{J}_2-\frac{g\mu_B}{2J_s}H_{c2}-\frac{2}{3}E_M, \tag{4}$$

$$\mathcal{J}_3=\mathcal{J}_2+\frac{g\mu_B}{6J_s}(H_{c2}-H_{c1})+\frac{1}{6}E_M,$$

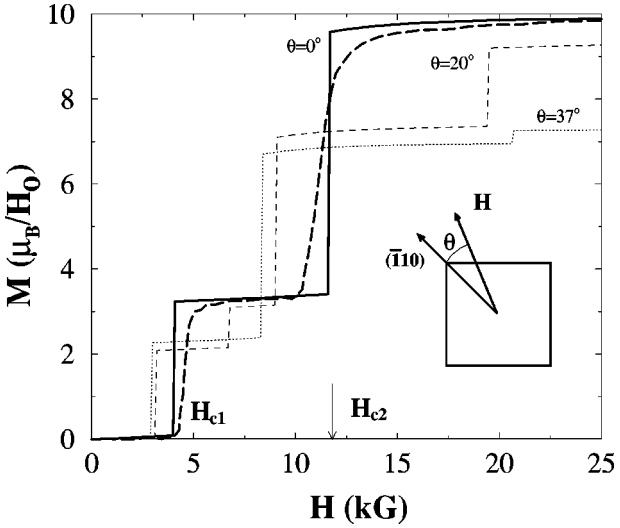

FIG. 1. Magnetization vs magnetic field for some representative angles θ between the field and the closest $\langle 110\rangle$ direction. For $\theta=0°$ the thick dashed line represents experimental data taken from Canfield *et al.* (Ref. 12). and the thick continuous line give results of our calculation. The two experimental parameters entering our model are the transition fields of the two metamagnetic transitions $H_{c1}=4.1$ kG and $H_{c2}=11.1$ kG. This figure should be compared with Fig. 1(a) of Ref. 12.

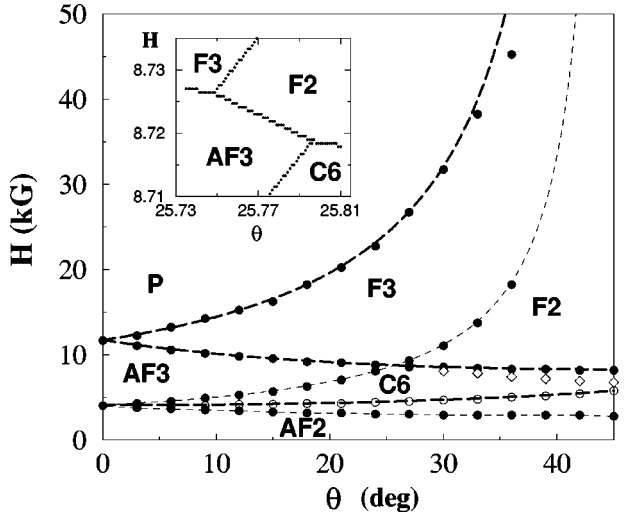

FIG. 2. Field vs. angle metamagnetic phase diagram for T = 2 K. The filled dots are calculated within our model and indicate the phase transitions where a sensible jump in the magnetization is seen ($\Delta M>0.2\mu_B$/Ho). The thick dashed lines are given in Ref. 12 as the best fit of the experimental data. Their functional form is $H^0_{c3}/\sin(45°-\theta)$, $H^0_{c2}/\cos(45°-\theta)$, and $H^0_{c1}/\cos\theta$. The values we used for the proportionality constants are $H^0_{c3}=H^0_{c2}=8.4$ kG and $H^0_{c1}=4.1$ kG. The two additional thin curves refer to the phase boundaries not yet observed in the experiments. Empty symbols refer to the stability of the AF3 phase with respect to AF2 (circles) and F2 (diamonds). The apparent tetracritical point in the phase diagram is composed of two very close usual tricritical points (inset).

where $E_M=2\pi(g\mu_B)^2/V_c=8.1\times10^{-3}$ meV comes from the contribution of the magnetization to the HFE. They assure that the relative stability of the three phases for $\theta=0°$ is the observed one. In order to use the easiest possible model, we set $\mathcal{J}_3=0$, which implies $\mathcal{J}_1=-8.0\times10^{-3}$ meV and $\mathcal{J}_2=-2.4\times10^{-3}$ meV. The final freedom in the model is the parameter $\mathcal{J}_0$, which works basically as a self-interaction and cannot be extracted starting from the energy differences among magnetic structures. We use $\mathcal{J}_0=4.8\times10^{-3}$ meV in order to have the transition between the paramagnetic and the incommensurate state at the experimental value T = 6 K.[4] Moreover, this choice make the internal molecular field large enough ($\sim$15 kG) to maintain the moments close to the saturation regime, as required.

After the model has been defined and all its parameters fixed, we present now the numerical results of the complete self-consistent MF calculation for the field-angle phase diagram at T = 2 K. The starting values for $\langle\mathbf{J}_i\rangle$ in the iteration algorithm are a set of random numbers and the possible periods allowed are in the range from one to nineteen planes. Typical magnetization curves are evaluated and they are shown in Fig. 1. They refer to experimental geometries with different angles θ between the external field **H** and the closest magnetic easy axis $\langle 110\rangle$. The resulting metamagnetic phase diagram is presented in Fig. 2. It contains all the phases in Table I and it agrees remarkably well with the experimental one. In particular, all the transition lines show simple trigonometrical dependence as a function of the angle θ as well as the corresponding magnetization values at the plateaux. In all the regions where the stable phases are $AF2$, $AF3$, $F3$, and P, we observe remarkable quantitative agreement with the experimental data in Ref. 12. The main qualitative differences between our model and experiments is the presence of two additional phases, the $F2$ and the $C6$, whose magnetization is different from the reported ones. However, the strongest disagreement is in the region of relatively low field and high angles where experimentally the strongest hysteresis is found. Another minor point is the absence of direct $AF3$-P transition for $\theta\neq0°$. Experimentally, the direct transition is observed for small angles up to $\theta=6°$ in the Ho compounds, but seems to have a much wider range in the similar phase diagram of $DyNi_2B_2C$.[18] We would like to stress however that it is not possible to improve this phase diagram by simply refining the parameters for the RKKY interaction. For example, allowing for $\mathcal{J}_3\neq0$, it is possible to stabilize at low field an additional phase, which is a distorted helix structure with wavelength five, but no change appears in the phase transitions among the other phases. In addition, as explained before, the effect of further effective interactions with neighboring planes beyond the third one may be eliminated by proper redefinition of the $\mathcal{J}_i$ with $i<3$. Therefore, if the two phases $F2$ and $C6$ are not observed in the experiments, we have to conclude that additional interactions (i.e., magnetoelastic couplings) have to play a role in the stability of the magnetic phases in $HoNi_2B_2C$.

Starting from the same model, it is possible to analyze the zero-field behavior as a function of temperature. In principle, this requires some attention since the magnetic system is now embedded in a superconducting material. This implies important changes in the $\mathbf{q}\sim0$ region of the Fourier transform of the RKKY function,[19] but leaves the relevant $\mathbf{q}\sim\pi$ region almost unchanged. Relying on this fact and on experiments on doped nonsuperconducting materials such as $HoNi_{2-x}Co_xB_2C$, which show a magnetic behavior very

similar to the undoped superconducting one,[20,21] we will use our purely magnetic model for the description of the zero-field phase diagram. At the MF level the second-order phase transition between the paramagnetic state and an ordered structure is expected to occur at the **Q** vector for which the $\mathcal{J}(\mathbf{q})$ has its maximum. In our model, this corresponds to $Q_c = 0.78\ \pi$ in the $\langle 001 \rangle$ direction, not far from the experimental value $Q_{exp} = 0.91\pi$.[7] The helical state is preferred with respect to the longitudinal modulated structure due to the ab easy plane for the moments. This truly incommensurate structure can be the ground state of the system only as long as the average moment per ion is small enough, i.e., close to the transition temperature. Lowering the temperature the ordered state develops and the CEF part of the HFE, proportional to fourth and the sixth powers in $\langle \mathbf{J}_i \rangle$, force the structure to find a commensurate compromise. Because in the self-consistent MF treatment it is not possible to treat, at the same time, truly incommensurate structures and the CEF, we cannot observe the actual C-IC transition. However, at a temperature of T = 5.5 K there is observed a first-order transition from $AF2$ to a helical state of wavelength 17, where the moments no longer point only along the easy directions. This is a clear indication that the RKKY energy starts to become dominant with respect to the CEF potential and drives the system into a state whose wave number **Q** is closer to the maximum of the RKKY function. To obtain better quantitative agreement for the ordering wave number *and* for the temperature interval in which the incommensurate state is stable, the function $\mathcal{J}(\mathbf{q})$ has to be refined in the Q_c region by including further parameters.

In conclusion, we presented a microscopic model for the rare-earth borocarbide system $HoNi_2B_2C$ that explains the main reported features of the anisotropic magnetic and temperature phase diagrams. The minimal model to achieve a semiquantitative description of the complex magnetic behavior of the system needs to include realistic CEF and effective RKKY interaction among the planes. On the other hand, no influence of SC needs to be included in the determination of the magnetic structures observed.

We would like to thank W. Henggeler *et al.* for the data on the CEF states. A.A. would also like to thank M. Laad, P. De Los Rios, and B. Canals. This work was performed under DFG Sonderforschungsbereich 463.

[1] R. J. Cava *et al.*, Nature (London) **367**, 252 (1994).
[2] P. C. Canfield *et al.*, Physica C **230**, 397 (1994).
[3] T. E. Grigereit *et al.*, Phys. Rev. Lett. **73**, 2756 (1994).
[4] M. S. Lin *et al.*, Phys. Rev. B **52**, 1181 (1995).
[5] H. Eisaki *et al.*, Phys. Rev. B **50**, 647 (1994).
[6] A. I. Goldman *et al.*, Phys. Rev. B **50**, 9668 (1994).
[7] J. P. Hill *et al.*, Phys. Rev. B **53**, 3487 (1996).
[8] Comment to Ref. 3 by T. Vogt *et al.*, Phys. Rev. Lett. **75**, 2628 (1995), and the Reply by T. E. Grigereit *et al.*, *ibid.* **75**, 2629 (1995).
[9] K. D. D. Rathnayaka *et al.*, Phys. Rev. B **53**, 5688 (1996).
[10] H. Schmidt and H. F. Braun, Phys. Rev. B **55**, 8497 (1997).
[11] B. K. Cho *et al.*, Phys. Rev. B **53**, 2217 (1996).
[12] P. C. Canfield *et al.*, Phys. Rev. B **55**, 970 (1997).
[13] L. F. Mattheiss, Phys. Rev. B **49**, 13 279 (1994).
[14] J. Jensen and A. R. Mackintosh, *Rare Earth Magnetism* (Oxford Science Publications, New York, 1991).
[15] M. L. Kulić, A. I. Buzdin, and L. N. Bulaevskii, cond-mat/9707024 (unpublished).
[16] U. Gasser *et al.*, Z. Phys. B **101**, 345 (1996).
[17] L. D. Landau, E. M. Lifshitz and L. P. Pitaevskii, *Electrodynamics of Continuous Media* (Butterworth-Heinemann, Washington, DC, 1984).
[18] P. C. Canfield *et al.*, Physica C (to be published).
[19] P. W. Anderson and H. Suhl, Phys. Rev. **116**, 898 (1959).
[20] J. W. Lynn *et al.*, Phys. Rev. B **53**, 802 (1996).
[21] P. Allenspach *et al.*, Physica B **230-232**, 882 (1997).